# Characterization of Hydrodynamic Surface Interactions of *Escherichia coli* Cell Bodies in Shear Flow

Tolga Kaya and Hur Koser

*Electrical Engineering Department, Yale University, Post Office Box 208284, New Haven, Connecticut 06520-8284, USA*

(Received 13 May 2009; published 24 September 2009)

We experimentally demonstrate that nonflagellated *Escherichia coli* strains follow modified Jeffery orbits in shear flow near a surface. We fully characterize their Jeffery orbits as a function of their aspect ratios and distance from that surface. Thanks to the linearity of Navier-Stokes equations under low-Reynolds-number conditions, the hydrodynamic body-wall interactions described here can be superimposed with flagellar motility and Brownian motion to construct models that explain the full picture of bacterial motility near a surface under shear flow.

DOI: 10.1103/PhysRevLett.103.138103 PACS numbers: 87.17.Jj, 87.16.Qp, 87.18.Ed

Hydrodynamic surface effects provide a stabilizing influence on the trajectories of motile bacteria, keeping them near the surface despite constant disturbances from Brownian effects [1–3]. In the presence of flow, such hydrodynamic effects become even more prevalent [4,5]. They lead to cells aligning and swimming towards one direction under a wide range of flow conditions, ultimately allowing *Escherichia coli* (*E. coli*) to find quiescent routes to swim upstream [6]. A physical understanding of such phenomena requires simple hydrodynamic models that capture the interactions among the cell body, the flagellar bundle, the bounding surface, and the local flow. Linearity of fluid dynamics under low-Reynolds-number conditions enables the study of these hydrodynamic effects in simpler components that can later be combined via superposition. In this Letter, we focus on experimentally characterizing one such hydrodynamic component—namely, interactions between the rod-shaped bodies of *E. coli* and a bounding surface under shear flow.

Our understanding of this hydrodynamic problem builds on Jeffery's study of isolated ellipsoids immersed in simple shear flow within an unbounded, viscous, Newtonian fluid [7]. Jeffery showed that the angular motion of a prolate spheroid follows certain closed, periodic orbits that depend on the shear rate and the aspect ratio of the spheroid. Jeffery's analysis was later proven valid for any axisymmetric particle in shear flow, leading to the concept of an effective particle aspect ratio ($r_e$) derivable from measured orbit periods [8,9]. Subsequent theoretical and numerical studies established that Jeffery's analysis is also applicable to spheroids in quadratic flow profiles, with local shear rates evaluated at a given particle's center [10]. Further experimental studies revealed that for an individual axisymmetric particle with an aspect ratio of $r_p$, $r_e/r_p$ decreases with increasing $r_p$ [11]. Consideration of wall effects in this context is relatively recent [12–14]. Interestingly, it has been shown that rodlike particles in shear flow near a wall still undergo Jeffery orbits—albeit more slowly, corresponding to an increased $r_e/r_p$ ratio that varies with the distance of the particle's center from the wall [13,14]. Although it may be presumed that nonflagellated, rod-shaped bacteria will also be subject to modified Jeffery orbits in shear flow near a boundary, we are aware of no prior experimental work characterizing this phenomenon.

To investigate the hydrodynamic interactions between bacteria cell bodies and a bounding wall in shear flow, we fabricated single-inlet/single-outlet microfluidic devices using soft lithography [15], and subjected nonflagellated *E. coli* K12 derivatives (YK4116 [16]) to various laminar flow regimes. A glass slide was coated with a 30 $\mu$m layer of polydimethylsiloxane prior to attachment of the top mold to create an all polydimethylsiloxane microchannel [Fig. 1(a)]. In experiments, bacteria were harvested during their log phase, suspended in Luria-Bertani broth at room temperature and allowed to precipitate to the bottom surface of the channel. A sterile, equal-part mixture of Luria-Bertani broth and glycerol was then pumped into the microchannel with a calibrated syringe pump at flows ranging from 100 $\mu$l/min up to 3.5 ml/min (see supplementary information [17]). A Navier-Stokes solver in COMSOL MULTIPHYSICS was used to calibrate the vertical gradient of flow (henceforth called "shear rate," or $\gamma$) along the bottom surface (see supplementary information [17], Figs. S1 and S2). The mixture's high viscosity (10 mPa s) partly suppressed both translational and rotational Brownian motion, enabling an easier observation of hydrodynamic effects as the cells drifted through the field of view [typically, within a few seconds at lowest flow rates; Fig. 1(b)]. In addition, we observed no noticeable sedimentation of bacteria within the short observation window, owing, in part, to the high viscosity of this mixture. Cells were imaged from below through a 40× phase-contrast objective (numerical aperture = 0.65; depth of focus = ±2 $\mu$m) via a high-speed, high-resolution video camera at 60 frames/second. Resulting image sequences were analyzed offline in MATLAB. Positions of bacteria body centers did not change appreciably along either the $x$ or $z$ direction during observation

 

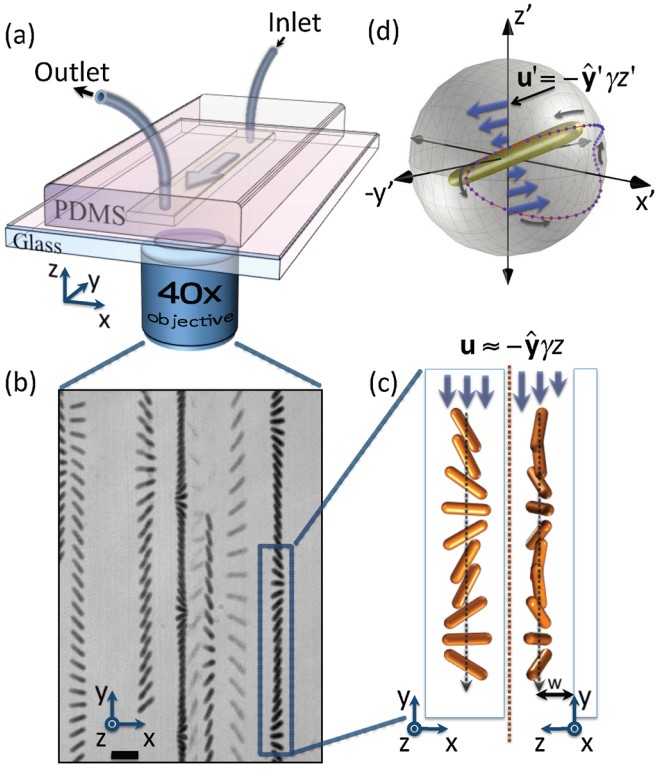


FIG. 1 (color online). Schematic representation of the experimental setup and a summary of observations. (a) *E. coli* were subjected to shear flow just over the bottom surface in a single-inlet single-outlet microfluidic device. (b) The position, orientation, and projected dimensions of the imaged cells were tracked as they drifted within the field of view of a 40× phase-contrast objective. Here, this composite image incorporates the minimum pixel value in every third frame within a 1.5 s observation window (scale bar: 5 $\mu$m). (c) Within the resolution of our experiment, a given bacterium's center appeared to follow a straight line along the downstream direction and parallel to the bottom surface. (d) Cells exhibited modified Jeffery orbits within the relative coordinate system that drifts with a given bacterium's center.

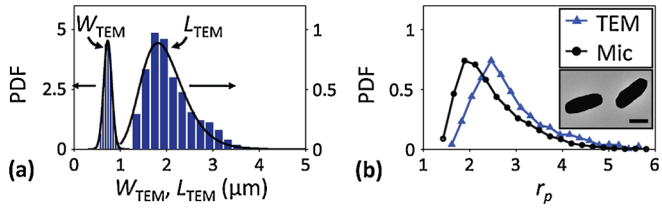


FIG. 2 (color online). Calibration of bacterial dimensions. (a) Probability density functions (PDFs) for bacteria dimensions were obtained using TEM images from 1213 individual, randomly selected bacteria. Cell widths were normally distributed (mean, $\mu = 0.74$ $\mu$m; standard deviation, $\sigma = 0.09$ $\mu$m), and bacteria lengths displayed a log-normal distribution ($\mu = 2.11$ $\mu$m, $\sigma = 0.56$ $\mu$m). (b) Cell body aspect ratios ($r_p$) observed under the light microscope ($\mu_{p,\mathrm{mic}} = 2.47$, $\sigma_{p,\mathrm{mic}} = 0.71$) were calibrated using TEM data ($\mu_{p,\mathrm{TEM}} = 2.87$, $\sigma_{p,\mathrm{TEM}} = 0.81$) via a simple transformation, $r_{p,\mathrm{TEM}} = r_{p,\mathrm{mic}}C + B$, where $C = \sigma_{\mathrm{TEM}}/\sigma_{\mathrm{mic}} = 1.13$ and $B = \mu_{\mathrm{TEM}} - C\mu_{\mathrm{mic}} = 0.08$. Inset depicts a typical TEM image of bacteria. The scale bar represents 0.8 $\mu$m.

[Fig. 1(c)]. Within a coordinate system that drifts with a given bacterium's center, the cells executed closed orbits [such as in Fig. 1(d)], as expected (see supplementary movies [17]).

Bacteria images obtained through phase-contrast light microscopy were inherently subject to diffraction effects. To accurately calibrate bacterial dimensions, we used transmission electron microscopy (TEM) images of cells harvested simultaneously with those imaged via light microscopy. Observed bacterial widths were narrowly Gaussian; cell body lengths displayed a log-normal distribution [Fig. 2(a)]. Cells suspended in Luria-Bertani broth at room temperature were sampled and characterized with TEM periodically, and their size distribution remained unchanged over the course of the experiment (up to six hours). We compared the distribution of $r_p$ values (defined as the ratio of body length to width) obtained from TEM images to apparent aspect ratios observed under the light microscope [Fig. 2(b)] [18]. An affine transformation, $r_{p,\mathrm{TEM}} = r_{p,\mathrm{mic}}C + B$, yielded the requisite calibration of the aspect ratios obtained from light microscopy images and shifted their distribution to virtually coincide with the TEM data. Here, $C = \sigma_{\mathrm{TEM}}/\sigma_{\mathrm{mic}}$ and $B = \mu_{\mathrm{TEM}} - C\mu_{\mathrm{mic}}$, such that the distribution of calibrated aspect ratios has the same mean ($\mu$) and standard deviation ($\sigma$) as those obtained from TEM images.

Figure 3(a) depicts the trajectory of a bacterium in the data set. We used periodic changes in the apparent length ($L$) of each bacterium during its Jeffery orbit [Fig. 3(b)] to estimate the angle $\alpha$ [Fig. 3(d)] between the $xy$ plane and the bacterium's principal axis. As a cell follows a particular Jeffery orbit with constant drift velocity [$v$ in Fig. 3(c)], it invariably passes through an orientation parallel to the bottom surface [$\alpha = 0$ in Fig. 3(d)]. In that instant, the apparent length of its image projected onto the $xy$ plane is at its maximum ($L_{\mathrm{max}}$). Hence, the ratio $L/L_{\mathrm{max}}$ can be used to reasonably estimate $\alpha$ through the inverse cosine of the ratio $L/L_{\mathrm{max}}$. Jeffery's original analysis may be adapted to include the axes defined in Fig. 1 and the angles $\psi$ and $\alpha$ depicted in Fig. 3 through a simple coordinate transformation (see supplementary information [17]). For a closed Jeffery orbit, $\alpha$ equals zero when the value of $\psi$ is at either extreme. By simply using either $\psi$ extremum (when $\alpha = 0$) as an initial condition to a Jeffery's orbit, the orbital trajectory of that cell can be fit rather well [Fig. 3(d) and 3(e)]. In Fig. 3, we have deliberately chosen to depict a slightly asymmetrical cell, which displays a corresponding mismatch in the length of any two consecutive half periods of its Jeffery orbit. In such cases, we included the cell's full average period in the data set.

It is important to note here that, as long as an individual cell remained within the same closed Jeffery orbit, its drift

velocity [e.g., $v$ in Fig. 3(c)] remained constant, indicating that the height ($w$) of the cell center from the surface was independent of bacterial orientation. Interestingly, this observation held true for all heights observed, even when either end of a given cell almost touched the surface. If bacteria bodies could be hydrodynamically approximated as linear concatenations of spheres whose diameters are given by the cell width ($W$) [19], then one would expect the presence of the bottom surface to have a noticeable effect on the average drift speed of the spheres [20] for $w/(W/2) < 2$, i.e., for $w < 0.58$ $\mu$m. As long as this condition is satisfied, we assume that $w$ may be approximated as $v/\gamma$. In the ensuing analysis, we included only those cells that displayed closed Jeffery orbits, and for which average $v/\gamma$ was 0.7 or greater. We excluded "pole-vaulting" [13] cells (i.e., those whose drift velocity increased as their height from the surface rose).

In the absence of Brownian motion, the period of an ideal Jeffery orbit is given by $T = 2\pi/\gamma\ (r_e + 1/r_e)$ [7]. The effective aspect ratio ($r_e$) can then be derived as

$$r_e = \frac{T\gamma}{4\pi} \mp \sqrt{\left(\frac{T\gamma}{4\pi}\right)^2 - 1} \qquad (1)$$

For prolate axisymmetric microparticles such as *E. coli* cell bodies, the square-root term in (1) is additive.

Measuring cell body periods at various shear rates revealed that the quantity $T\gamma$ was constant for a given set of $r_p$ and $w$ values, as expected [Fig. 4(a)]. We found that $r_e/r_p$ increased (i.e., orbital period was longer for a given

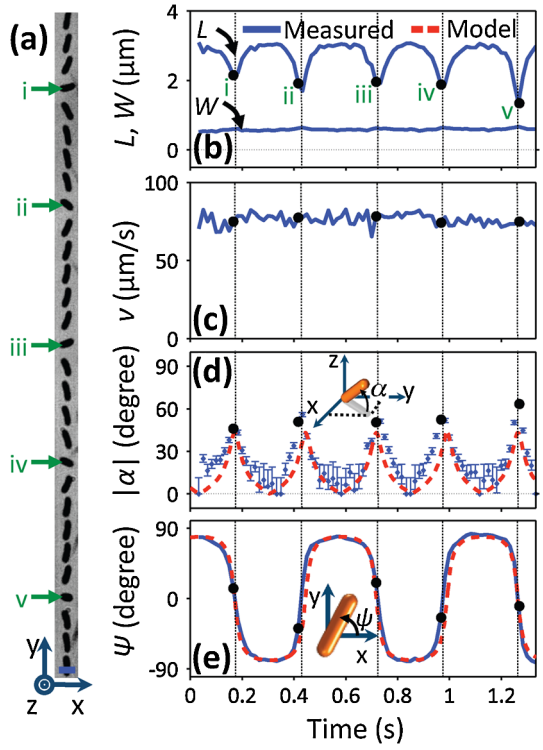


FIG. 3 (color online). Calculation of trajectory parameters for an individual bacterium. (a) Trajectory of a slightly asymmetric bacterium in a shear rate of 65.6 $s^{-1}$ as observed through light microscopy. For clarity, this composite image incorporates the minimum pixel value in every third frame, depicting the same bacterium in 50 ms intervals within a 1.4 s observation window (scale bar: 1.8 $\mu$m). Snapshots (i) through (v) are depicted in (b)–(e) as circles. (b) Bacterium's projected length ($L$) varies between 3.6 $\mu$m ($L_{max}$) and about 2 $\mu$m, whereas its apparent width ($W$) is virtually constant at 1.2 $\mu$m. Apparent aspect ratio for this individual bacterium is 2.96. (c) The average drift velocity ($v$) of the bacterium fluctuates no more than 7% about a constant mean; most of this fluctuation originates from the inherent uncertainty associated with determining the position of the bacterium's center from pixelated images. (d) The angle $\alpha$ (deduced from $L_{max}$ and instantaneous $L$) reaches its maxima whenever the orientation angle ($\psi$) of the bacterium in the $xy$ plane crosses 0 (e), as depicted with the vertical grid lines. Because of the slight shape asymmetry of the bacterium, one half of its Jeffery orbit is longer than the other. The overall orbital period is 0.54 s.

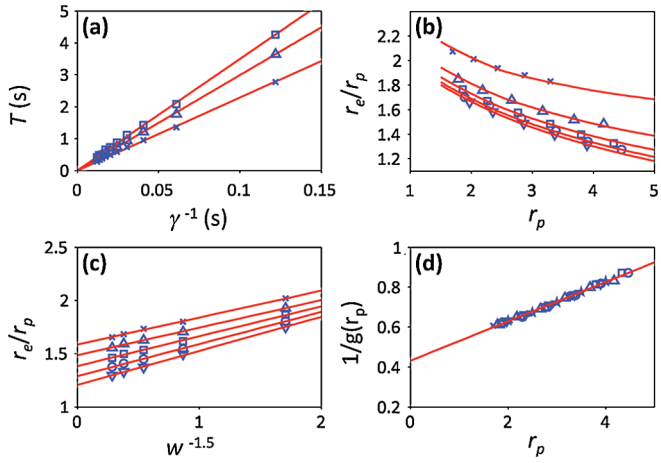


FIG. 4 (color online). Characterization of hydrodynamic surface interactions of 13 284 cell bodies in shear flow. (a) At fixed $w$ (1.49 $\mu$m), $T\gamma$ is constant (22.98, 29.92, and 34.99) for a narrow range ($\pm 1\%$) of $r_p$ values (centered around 2.0, 3.0, and 4.0, respectively), as expected. Minimum $R$-squared value among the three linear fits is 0.997. (b) $r_e/r_p$ increases as $r_p$ and $w$ get smaller. Here, $w = 0.7 \pm 0.2$ $\mu$m (x marks), $w = 1.1 \pm 0.2$ $\mu$m (triangles), $w = 1.5 \pm 0.2$ $\mu$m (squares), $w = 1.9 \pm 0.2$ $\mu$m (circles), and $w = 2.3 \pm 0.2$ $\mu$m (down triangles). (c) $r_e/r_p$ vs $w^{-1.5}$ reveals straight lines (minimum $R$-squared value, 0.998) for different average $r_p$ values: $r_p = 2$ (x marks), $r_p = 2.5$ (triangles), $r_p = 3$ (squares), $r_p = 3.5$ (circles), and $r_p = 4$ (down triangles). The slopes of the fits correspond to $f(r_p)$ in Eq. (2). (d) Combining fitted data from (b) and (c), we find that $1/g(r_p)$, as defined in Eq. (2), is linear ($R$-squared value, 0.996) with $r_p$ for all $w$ values: $w = 0.7 \pm 0.2$ $\mu$m (x marks), $w = 1.1 \pm 0.2$ $\mu$m (triangles), $w = 1.5 \pm 0.2$ $\mu$m (squares), $w = 1.9 \pm 0.2$ $\mu$m (circles), $w = 2.3 \pm 0.2$ $\mu$m (down triangles), and as $w$ goes to infinity (pentagrams). The slope and the intercept of the linear fit are found to be 0.099 and 0.431, respectively.

shear rate) for smaller values of either $r_p$ or deduced $w$ [Fig. 4(b)]; this finding is consistent with previous literature on prolate fibers [13,14]. In an effort to deduce a simple, empirical relationship to fit to the results in Fig. 4(b), we assume that $r_e/r_p$ takes the form

$$\frac{r_e}{r_p} = f(r_p)w^{-n} + g(r_p) + k, \tag{2}$$

where $f(r_p)$ and $g(r_p)$ are general functions of $r_p$, and $k$ is a constant. One could linearly interpolate between the different $r_p$ data points of Fig. 4(b) to deduce $r_e/r_p$ for different fixed values of $r_p$. We have found that $n = 1.5$ gives the best linear relationship between $r_e/r_p$ and $w^{-n}$ for a given $r_p$ value [Fig. 4(c)]. The slopes of the linear fits in Fig. 4(c) correspond to $f(r_p)$ values (depicted in Fig. S4 [17]); a simple third order polynomial that fits these values well within the considered $r_p$ range (2.0–4.0) is given by

$$f(r_p) \approx -0.01r_p^3 + 0.13r_p^2 - 0.36r_p + 0.57. \tag{3}$$

The $y$ intercepts in Fig. 4(c) correspond to the limit when $w$ goes to infinity (i.e., bacteria in unbounded shear flow). We have determined that $1/g(r_p) = [r_e/r_p - f(r_p)w^{-1.5} - k]^{-1}$ vs $r_p$ can be fit with the same straight line for all $w$ values (including infinity) when $k = 0$. From Fig. 4(d), we deduce that

$$\frac{r_e}{r_p} = f(r_p)w^{-1.5} + \frac{1}{c + dr_p}, \tag{4}$$

where $c = 0.429$ and $d = 0.099$. This empirical formula fits well to the overall data listed in Fig. 4(b) (solid lines). Our attempts to exploit different possibilities for $g(r_p)$ and $k$ in (2) have not resulted in a consistent fit that could incorporate a finite limit for $r_e/r_p$, as suggested in [13]. We note that our observations with *E. coli* are limited to their relatively small aspect ratios, and extrapolating from this data set to very large $r_p$ values may not necessarily be warranted.

In summary, we have experimentally demonstrated that nonflagellated *E. coli* strains follow modified Jeffery orbits in shear flow near a surface. We have determined that, given a shear rate, hydrodynamic interactions of bacterial cell bodies with the surface are fully characterized by their aspect ratios and their separation from that surface. A main goal of this Letter has been to measure and characterize this hydrodynamic phenomenon, as an important first step in modeling and understanding shear-assisted orientation and upstream migration of motile *E. coli* [6]. Thanks to the linearity of Navier-Stokes equations under low-Reynolds-number conditions, the hydrodynamic body-wall interactions described here can be superimposed with flagellar motility and Brownian motion to model and explain the full picture of bacterial motility near a surface under shear flow.

We thank J. McMurry for bacteria strains. T. Mahadevan and B. Fischer helped with TEM measurements.

[1] E. Lauga, W. R. DiLuzio, G. M. Whitesides, and H. A. Stone, Biophys. J. **90**, 400 (2006).
[2] A. P. Berke, L. Turner, H. C. Berg, and E. Lauga, Phys. Rev. Lett. **101**, 038102 (2008).
[3] G. Li, L.-K. Tam, and J. X. Tang, Proc. Natl. Acad. Sci. U.S.A. **105**, 18 355 (2008).
[4] W. R. DiLuzio, L. Turner, M. Mayer, P. Garstecki, D. B. Weibel, H. C. Berg, and G. M. Whitesides, Nature (London) **435**, 1271 (2005).
[5] C. Pozrikidis, J. Fluid Mech. **541**, 105 (2005).
[6] J. Hill, O. Kalkanci, J. L. McMurry, and H. Koser, Phys. Rev. Lett. **98**, 068101 (2007).
[7] G. B. Jeffery, Proc. R. Soc. A **102**, 161 (1922).
[8] F. P. Bretherton, J. Fluid Mech. **14**, 284 (1962).
[9] H. L. Goldsmith and S. G. Mason, J. Colloid Sci. **17**, 448 (1962).
[10] A. T. Chwang, J. Fluid Mech. **72**, 17 (1975).
[11] B. J. Trevelyan and S. G. Mason, J. Colloid Sci. **6**, 354 (1951).
[12] S. Yamamoto and T. Matsuoka, J. Chem. Phys. **102**, 2254 (1995).
[13] C. A. Stover and C. Cohen, Rheol. Acta **29**, 192 (1990).
[14] P. Skjetne, R. F. Ross, and D. J. Klingenberg, J. Chem. Phys. **107**, 2108 (1997).
[15] Y. Xia and G. M. Whitesides, Angew. Chem., Int. Ed. Engl. **37**, 550 (1998).
[16] Y. Komeda, K. Kutsukake, and T. Iino, Genetics **94**, 277 (1980).
[17] See EPAPS Document No. E-PRLTAO-103-027940 for supplementary information and movies. For more information on EPAPS, see http://www.aip.org/pubservs/epaps.html.
[18] Since light microscopy images of bacteria are projections on the $xy$ plane, the apparent length of a given bacterium changes periodically during its Jeffery orbit, whereas its apparent width at its center remains unchanged [see Fig. 3(b)]. To calculate $r_p$ from light microscopy images (i.e., $r_{p,\mathrm{mic}}$), the average width at the center of the cell and the maximum apparent length during at least one half period of the Jeffery orbit were selected.
[19] S. Yamamoto and T. Matsuoka, J. Chem. Phys. **98**, 644 (1993).
[20] A. J. Goldman, R. G. Cox, and H. Brenner, Chem. Eng. Sci. **22**, 653 (1967).